RSC Advances

RSC Publishing

PAPER

View Article Online
View Journal | View Issue

Cite this: *RSC Advances*, 2013, **3**, 12743

Effects of hydrophobic hydration on polymer chains immersed in supercooled water

Tomonari Sumi*[a] and Hideo Sekino[b]

A multiscale simulation of a hydrophobic polymer chain immersed in water including the supercooled region is presented. Solvent effects on the polymer conformation were taken into account *via* liquid–state density functional theory in which a free-energy functional model was constructed using a density response function of bulk water, determined from a molecular dynamics (MD) simulation. This approach overcomes sampling problems in simulations of high-viscosity polymer solutions in the deeply supercooled region. Isobars determined from the MD simulations of 4000 water molecules suggest a liquid–liquid transition in the deeply supercooled region. The multiscale simulation reveals that a hydrophobic polymer chain exhibits swelling upon cooling along isobars below a hypothesized second critical pressure; no remarkable swelling is observed at higher pressures. These observations agree with the behavior of a polymer chain in a Jagla solvent model that qualitatively reproduces the thermodynamics and dynamics of liquid water. A theoretical analysis of the results obtained from the multiscale simulation show that a decrease in entropy due to the swelling arises from the formation of a tetrahedral hydrogen bond network in the hydration shell.

Received 19th March 2013,
Accepted 3rd May 2013

DOI: 10.1039/c3ra41320a

www.rsc.org/advances

1. Introduction

Water in the liquid phase exhibits (i) a thermodynamic anomaly (density decrease upon cooling and entropy increase with pressurization) and (ii) a dynamic anomaly (increase in diffusivity upon compression).[1,2] These anomalies are related to the tetrahedral structure of the hydrogen bond network. It has been hypothesized that in the deeply supercooled region, water undergoes a phase transition from a low-density liquid (LDL) state, with a large amount of empty space around the tetrahedrally coordinated molecules, to a high-density liquid (HDL) state in which the tetrahedral structure is distorted and weakened, whereby the empty space decreases.[3–5] The possible existence of the liquid–liquid critical point is experimentally supported by the changing gradient of the metastable melting curves observed for different ice polymorphs.[6,7] These two different dense liquids have well characterized counterparts in the glassy state: the low-density and high-density amorphous ice forms.[8,9]

Recently it was shown that a spherically symmetric two-scale potential liquid model (Jagla model)[10,11] with both repulsive and attractive ramps not only exhibits thermodynamic and dynamic anomalies similar to those found in liquid water as well as the liquid–liquid transition,[12–14] but also reproduces water-like solvation thermodynamics such as a decrease in the solubility of small non-polar solutes with decreasing temperature.[15] These observations strongly suggest that these anomalies may arise from the hypothesized liquid–liquid transition in the deeply supercooled state of water.[3,16] Moreover, it was demonstrated that the two-ramp spherically symmetric Jagla solvent model, at which particles interacting *via* a hard core repulsion ($r_1 = d_{hc}$) and a soft core repulsion ($r_2 = 1.72d_{hc}$) and an attraction ($r_3 \leqslant 3d_{hc}$) [see Fig. 1(a) in ref. 15], exhibits a significant swelling of a solvophobic polymer chain upon cooling.[15,17] It has also been pointed out that the phenomenon might be related to the basis of cold denaturation of proteins.

The study presented here is the third work in a series of studies on water and hydration effects over a wide range of pressures and temperatures. The first study was conducted to investigate the underlying physical mechanisms of high-pressure unfolding of proteins from a general point of view of hydrophobic hydration effects.[18] In the second work, extensive molecular dynamics simulations of water were performed over a wide range of temperatures and pressures including the hypothesized liquid–liquid transition in the deeply supercooled state, and a generalized Arrhenius analysis of the self-diffusion coefficient of bulk water was presented.[19] A rigid planar four-site interaction potential model of water TIP4P/2005[20] was employed in these studies to determine the thermodynamic and dynamic properties of bulk water. In the study presented here, we performed a multiscale simulation of hydrophobic polymer chains immersed in water to investigate the relationship between the thermodynamic anomalies of

[a]*Department of Chemistry, Okayama University, 3-1-1 Tsushima-Naka, Kita-ku, Okayama 700-8530, Japan. E-mail: sumi@okayama-u.ac.jp*
[b]*Department of Computer Science and Engineering, Toyohashi University of Technology, Tempaku-cho, Toyohashi 441-8580, Japan*

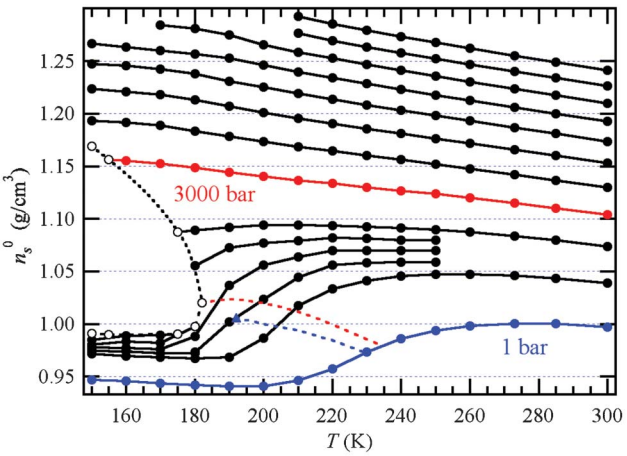

Fig. 1 Number densities (solid circles) as a function of temperature for various isobars in the density–temperature plane. Isobars, from bottom to top in the figure, are shown for 1, 1000, 1250, 1500, 1750, 2000, 3000, 4000, 5000, 6000, 7000, 8000, 9000, and 10 000 bar. Densities along the 1250, 1500, and 1750 isobars are given only for temperatures lower than 250 K. The open circles connected by the dashed black line show hypothesized coexistent densities that were estimated from the densities determined from the MD simulations (shown by the solid circles) assuming that these isobars indicate the liquid–liquid transition between the high-density liquid (HDL) and the low-density liquid (LDL) states. The dashed red line is the maximum of the isothermal compressibility κ_T. The hypothesized second liquid–liquid critical point that was estimated from these isobars and the maximum κ_T are located at T_c = 182 K, n_c^0 = 1.02 g cm^{-3}, and 1580–1620 bar. The dashed blue line and blue triangle indicate the maximum κ_T and the hypothesized second liquid–liquid critical point determined by Abascal and Vega (ref. 28), respectively.

water and hydration thermodynamics. In this method, the solvation effects are taken into account *via* an effective Hamiltonian[21] that is constructed from a density functional model in which a solvent density–response function and a polymer–solvent pair correlation function are determined from a molecular dynamics (MD) simulation of bulk water and a density functional theory (DFT)-based integral equation for polymer–solvent mixtures, respectively.

The outline of this paper is as follows. The details of the theory and computation of the multiscale simulation of the polymer chain in solvent are presented in Sec. 2 and 3, respectively. In Sec. 4, we present and discuss the results obtained from both the MD simulations of bulk water and the multiscale simulations of the polymer chain in water. A summary is given in Sec. 5.

2. Multiscale simulation of polymer chains in solvent

From a partition function of infinitely diluted polymer solutions, the following effective Hamiltonian for a polymer chain immersed in solvent can be derived using DFT:[21]

$$H_{\mathrm{eff}}\left(\left\{\mathbf{r}_1^{\lambda}\right\}\right)=H_{\mathrm{ipc}}\left(\left\{\mathbf{r}_1^{\lambda}\right\}\right)+\sum_{a=1}^{N_{\mathrm{p}}}\sum_{b=1}^{N_{\mathrm{p}}}W_{\mathrm{pp}}\left(\left|\mathbf{r}_1^{a}-\mathbf{r}_1^{b}\right|\right), \quad (1)$$

where $H_{\mathrm{ipc}}\left(\left\{\mathbf{r}_1^{\lambda}\right\}\right)$ is a Hamiltonian for the polymer chain existing in a vacuum, N_{p} is the number of monomers, and $W_{\mathrm{pp}}(r)$ is a solvent-induced interaction between monomers. The effective Hamiltonian provided by eqn (1) should approximately reproduce the ensemble average of the conformational properties of the polymer chain provided by the original partition function; effects of the solvent on the conformational properties are reproduced by $W_{\mathrm{pp}}(r)$. From the density functional Taylor expansion of the grand potential for the solvent $\Omega_{\mathrm{s}}[U_{\mathrm{sp}}^{\mathrm{pr}}]$ under an external field $U_{\mathrm{sp}}^{\mathrm{pr}}\left(\left\{\mathbf{r}_1^{\lambda}\right\}\right)$ up to the second order, and making a site decomposition assumption, the Fourier transform of $W_{\mathrm{pp}}(r)$ is obtained as follows:[21]

$$\hat{W}_{\mathrm{pp}}(k)=k_{\mathrm{b}}T\hat{\sigma}_{\mathrm{pp}}^{-1}(k)\hat{h}_{\mathrm{ps}}(k)n_{\mathrm{s}}^{0}\hat{C}_{\mathrm{ss}}(k)n_{\mathrm{s}}^{0}\hat{h}_{\mathrm{sp}}(k)\hat{\sigma}_{\mathrm{pp}}^{-1}(k)/2. \quad (2)$$

Here, the external field $U_{\mathrm{sp}}^{\mathrm{pr}}\left(\left\{\mathbf{r}_1^{\lambda}\right\}\right)$ for $\Omega_{\mathrm{s}}[U_{\mathrm{sp}}^{\mathrm{pr}}]$ in the original partition function is caused by the monomer–solvent interaction potential $v_{\mathrm{ps}}(r)$, where the conformation of the polymer chain is fixed in space with a set of coordinates for the monomer positions $\{\mathbf{r}_1^{\lambda}\}$. In eqn (2), k_{b} is the Boltzmann constant, T is the temperature, and n_{s}^{0} is the number density of the solvent. The terms $\hat{\sigma}_{\mathrm{pp}}(k)$, $\hat{h}_{\mathrm{ps}}(k)$, and $\hat{C}_{\mathrm{ss}}(k)$ are Fourier transforms of the intramolecular correlation function, polymer–solvent pair correlation function, and direct correlation function between the solvents, respectively. The solvation structure around the polymer chain characterized by $h_{\mathrm{ps}}(r)$ and the equilibrium average conformation of the polymer chain characterized by $\sigma_{\mathrm{pp}}(r)$ influence each other. Therefore, both the correlation functions $h_{\mathrm{ps}}(r)$ and $\sigma_{\mathrm{pp}}(r)$ should ideally be determined in a self-consistent manner.

Here, $C_{\mathrm{ss}}(r)$ (or $h_{\mathrm{ss}}(r)$) and $h_{\mathrm{ps}}(r)$ in eqn (2) were determined from integral equations based on DFT for polymer–solvent mixtures[21] using $\sigma_{\mathrm{pp}}(r)$ as the input. In the limit of infinitely diluted polymer solutions, the DFT for polymer–solvent mixtures that is formulated for an arbitrary concentration of the polymer chain provides an integral equation for $h_{\mathrm{ss}}(r)$ in the bulk pure solvent, which is independent of the integral equation for $h_{\mathrm{ps}}(r)$. This is a general conclusion that is driven from statistical mechanics in the limit of infinitely diluted solutes. The reason why $h_{\mathrm{ss}}(r)$ in the polymer–solvent mixture is equal to $h_{\mathrm{ss}}(r)$ for the bulk solvent is that the number of solvent particles in the solvation shell around the solutes is finite in comparison with the infinite number of non-perturbation solvent particles in the case of infinitely diluted solutions. However, the equivalence in these $h_{\mathrm{ss}}(r)$ values does not indicate that the correlation between solvents in the solvation shell are not perturbed by solutes in the limit of infinitely diluted solutions. The DFT for the polymer–solvent mixtures provides the following integral equation for $h_{\mathrm{ps}}(r)$:[21]

$$h_{\mathrm{ps}}(r)=\int\left\{\prod_{a=1}^{N_{\mathrm{p}}}\mathrm{d}\mathbf{r}_1^{a}\right\}\left\{\frac{1}{N_{\mathrm{p}}}\sum_{a=1}^{N_{\mathrm{p}}}\delta\left(\left|\mathbf{r}-\mathbf{r}_1^{a}\right|\right)\right\}\left\{\prod_{a=1}^{N_{\mathrm{p}}-1}s\left(\left|\mathbf{r}_1^{a}-\mathbf{r}_1^{a+1}\right|\right)\right\}\left\{\prod_{a=1}^{N_{\mathrm{p}}}\exp\left(-\boldsymbol{\beta}U_{\mathrm{p}}^{\mathrm{ref}}\left(\left|\mathbf{r}_1^{a}\right|\right)\right)\right\}-1, \quad (3)$$

where

$$U_{\mathrm{p}}^{\mathrm{ref}}(r) = v_{\mathrm{ps}}(r) - \frac{1}{\beta}\int \mathrm{d}\mathbf{k}\exp(-i\mathbf{k}\cdot\mathbf{r})\hat{\Gamma}_{\mathrm{p}}(k), \quad (4)$$

$$\hat{\Gamma}_{\mathrm{p}}(k) = \frac{\hat{\sigma}_{\mathrm{pp}}(k) - \hat{\sigma}_{\mathrm{pp}}^{\mathrm{ref}}(k)}{\hat{\sigma}_{\mathrm{pp}}(k)\hat{\sigma}_{\mathrm{pp}}^{\mathrm{ref}}(k)}\hat{h}_{\mathrm{ps}}(k) + \frac{\hat{h}_{\mathrm{ps}}(k)}{\hat{\sigma}_{\mathrm{pp}}(k)} n_{\mathrm{s}}^{0}\hat{C}_{\mathrm{ss}}(k). \quad (5)$$

In eqn (3), $s(r)$ is a bond function between nearest-neighbor monomers and is given by $\delta(L_{\mathrm{pp}} - r)/4\pi L_{\mathrm{pp}}^2$, where L_{pp} is the bond length. Eqn (3) corresponds to the monomer density distribution function of an ideal chain gas under the effective external field $U_{\mathrm{p}}^{\mathrm{ref}}(r)$. The ideal chain gas, in which there are no interactions except for the bonding interaction between nearest-neighbor monomers, is introduced as a reference system in the DFT for the polymer–solvent mixtures. In eqn (5), $\hat{\sigma}_{\mathrm{pp}}^{\mathrm{ref}}(k)$ is the Fourier transform of the intramolecular correlation function for the ideal chain, *i.e.*, the reference system. As mentioned above, the direct correlation function for the bulk solvent is denoted as $\hat{C}_{\mathrm{ss}}(k)$ in eqn (5). However, this theoretical conclusion does not necessarily indicate that the perturbation effects from solutes on the correlation between solvents in the solvation shell are not taken into account in the integral equation approach.

The multiscale simulation for the polymer chain in a solvent consists of the following two parts: (i) a single-polymer simulation with the effective Hamiltonian of eqn (1) and (2), which is needed to determine $\sigma_{\mathrm{pp}}(r)$, and (ii) solving the integral equations for $h_{\mathrm{ss}}(r)$ and $h_{\mathrm{ps}}(r)$ given by eqn (3)–(5), where $\sigma_{\mathrm{pp}}(r)$ is used as the input. Both (i) and (ii) are performed iteratively to determine self-consistent forms of $\sigma_{\mathrm{pp}}(r)$ and $h_{\mathrm{ps}}(r)$. The approximations introduced in the derivation of eqn (1)–(5) have been demonstrated to predict high-pressure unfolding of hydrophobic polymer chains[18] as well as high-temperature and low-pressure unfolding of solvophobic polymer chains.[22]

3. Computational details

To perform the multiscale simulation using eqn (1)–(5), we need the structure factor of bulk water $S_{\mathrm{ss}}(k)$ to construct the DF model for water in eqn (2), (4), and (5) because $\hat{C}_{\mathrm{ss}}(k)$ is obtained from $\hat{C}_{\mathrm{ss}}(k) = [1 - S_{\mathrm{ss}}^{-1}(k)]/n_{\mathrm{s}}^{0}$.(ref. 23) Here we employ the following approach to determine $S_{\mathrm{ss}}(k)$: An MD simulation of bulk water is performed first to calculate the radial distribution function between oxygen sites $g_{\mathrm{ss}}(r)$. We then extend this $g_{\mathrm{ss}}(r)$ function to a large radial distance (50 nm) using the HNC integral equation;[23] the $g_{\mathrm{ss}}(r)$ values for $r \leqslant r_{\mathrm{h}}$ (1.3–1.7 nm) were fixed to the MD values when iteratively solving the HNC integral equation $g_{\mathrm{ss}}(r) = h_{\mathrm{ss}}(r) + 1 = \exp[h_{\mathrm{ss}}(r) - C_{\mathrm{ss}}(r)]$ for $r > r_{\mathrm{h}}$,[24] where the intermolecular potential is assumed to be neglible for $r > r_{\mathrm{h}}$. The r_{h} value was chosen carefully so that the $g_{\mathrm{ss}}(r)$ obtained from the HNC integral equation for $r > r_{\mathrm{h}}$ was smoothly connected to the $g_{\mathrm{ss}}(r)$ determined from the MD simulation for $r \leqslant r_{\mathrm{h}}$. Here, we note that the statistical error included in the MD values of $g_{\mathrm{ss}}(r)$ gradually increases as the radial distance increases. This error would artificially influence the result of $g_{\mathrm{ss}}(r)$ obtained from the integral equation. If the structural information for larger radial distances without the statistical error were taken into account by choosing an appropriate value of r_{h} when the integral equation was solved, the extended values of $g_{\mathrm{ss}}(r)$ determined from the integral equation would almost agree with the MD values of $g_{\mathrm{ss}}(r)$ at radial distances around r_{h} for $r > r_{\mathrm{h}}$. In general, it is known that the bridge function that gives an exact correction for the HNC approximation is a short-range function.[23] Since all the bridge corrections are already taken into account through the radial distribution function determined from the MD simulation for $r \leqslant r_{\mathrm{h}}$, the approach using the HNC integral equation can extend the radial distribution function to $r > r_{\mathrm{h}}$ at quite a high precision. Therefore, we can obtain an accurate $S_{\mathrm{ss}}(k)$ by combining the MD result of $g_{\mathrm{ss}}(r)$ and the HNC integral equation.

In this study, a rigid planar four-site interaction potential model of water TIP4P/2005[20] was employed for the MD simulation of bulk water. All the MD simulations were performed for 4000 water molecules in the isothermal–isobaric *NpT* ensemble using the MD package GROMACS 4.0.5.[25] The time step was 2 fs, and the cutoff distance of the Lennard–Jones (LJ) potential was 0.9 nm. The Coulomb interaction was treated by the particle–mesh Ewald method. Simulations of between 40 and 100 ns were conducted to evaluate the ensemble average of the thermodynamic quantities and $g_{\mathrm{ss}}(r)$.

For the multiscale simulation of the polymer chain in water, we employed a hydrophobic polymer model consisting of 512 monomers interacting *via* the LJ potential with a set of parameters $\varepsilon_{\mathrm{pp}}$ = 0.25 kcal mol^{-1} and d_{pp} = 0.38 nm. The nearest-neighbor monomers were linked *via* a rigid bond with a bond length $L = d_{\mathrm{pp}}$, where d_{pp} was the diameter of the monomer. The polymer chain model was also given an intrinsic stiffness by including a bond angle potential $u_{\mathrm{ang}}(\theta) = k_{\mathrm{ang}}(\theta - \theta_0)^2$, where θ is the angle between three consecutive monomers, and the equilibrium value was $\theta_0 = 109^\circ$. The value of k_{ang} was set to 2.5 kcal mol^{-1} rad^{-2}. For the LJ parameters between the polymer and water, the equations $\varepsilon_{\mathrm{ps}} = \sqrt{\varepsilon_{\mathrm{pp}}\varepsilon_{\mathrm{ss}}}$ and $d_{\mathrm{ps}} = (d_{\mathrm{pp}} + d_{\mathrm{ss}})/2$ were used, where $\varepsilon_{\mathrm{ss}}$ and d are 0.1852 kcal mol^{-1} and 0.31589 nm, respectively, from the TIP4P/2005 model of water.[20] The following Weeks–Chandler–Andersen (WCA) repulsion was employed as the monomer–solvent interaction: $v_{\mathrm{ps}}(r) = 4\varepsilon_{\mathrm{ps}}[(d_{\mathrm{ps}}/r)^{12} - (d_{\mathrm{ps}}/r)^{6}] + \varepsilon_{\mathrm{ps}}$ for $r \leqslant 2^{1/6}d_{\mathrm{ps}}$ and $v_{\mathrm{ps}}(r) = 0$ for $r > 2^{1/6}d_{\mathrm{ps}}$.

The smart Monte Carlo (SMC) method[26] was employed to evaluate the ensemble average with respect to the polymer conformation. The SMC simulation was performed under the effective Hamiltonian of the solvated polymer chain. The bond lengths were kept constant using the RATTLE algorithm of the TINKER simulation package.[27] The equilibrium properties were evaluated from an average of 2.5 $\times$ 10^6 MC steps. The integral equations were solved with 4096 grid points, in which the maximum value of the radial distance was 50 nm. Except for significant swelling states, 40 cycles between the SMC simulation with the effective Hamiltonian and solving the

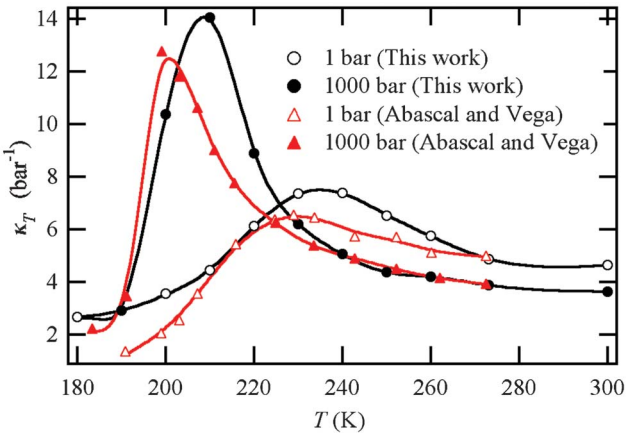

Fig. 2 Isothermal compressibility κ_T as a function of temperature along isobars. Lines are natural smoothing spline fit to the results. The open and solid black circles show results obtained from the compressibility equation $\kappa_T = S_{ss}(k = 0)/n_s^0 k_b T$, where $S_{ss}(k)$ is the structure factor at 1 and 1000 bar, respectively. The open and solid red triangles show the results of Abascal and Vega (ref. 28) at 1 and 1000 bar, respectively.

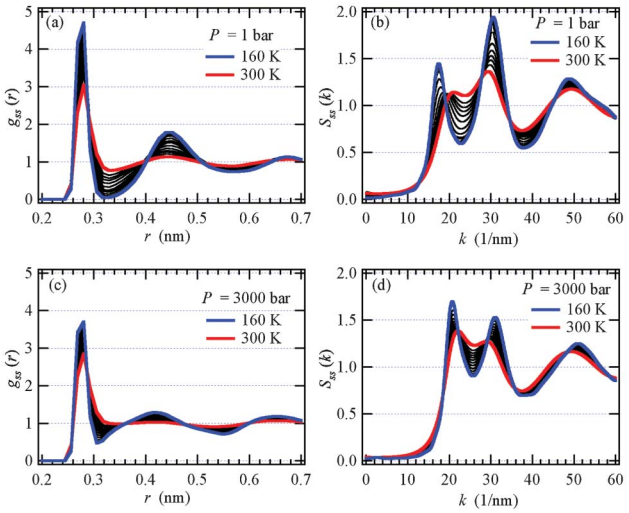

Fig. 3 Radial distribution function of the oxygen site $g_{ss}(r)$ and structure factor obtained from $S_{ss}(k) = 1 + n_c^0 \hat{h}_{ss}(k)$, where $\hat{h}_{ss}(k)$ is the Fourier transform of $h_{ss}(r) = g_{ss}(r) - 1$, and n_c^0 is the number density of water. Data for $g_{ss}(r)$ and $S_{ss}(k)$ are shown for temperatures of 160–300 K at (a) and (b) 1 bar, and (c) and (d) 3000 bar.

integral equation for $h_{ps}(r)$ were typically performed to evaluate the ensemble average of $\sigma_{pp}(r)$ and the radius of gyration R_g.

4. Results and discussions

In Fig. 1, isobars are shown as a function of temperature in the density–temperature plane. The solid circles indicate number densities determined from the MD simulation. Isobars are shown for pressures of 1 to 10 000 bar from the bottom to the top. The open circles connected by the dashed black line, estimated from the MD densities, illustrate the hypothesized coexistence line of a liquid–liquid transition between the HDL and LDL. The dashed red line crossing the isobars is the maximum of the isothermal compressibility, κ_T. The location of the second liquid–liquid critical point C^* was estimated from the schematic coexistent line and the maximum of κ_T to be located at T_c = 182 K, n_c^0 = 1.02 g cm^{-3}, and between 1580 and 1620 bar. The maximum of κ_T, *i.e.*, the Widom line in the case of a liquid–liquid transition, determined from the thermodynamic limit of the 4000-water-molecule MD result using the integral equation almost agrees with the Widom line determined by Abascal and Vega from the volume fluctuation of a 500-water-molecule MD simulation[28] using the TIP4P/2005 model. However, our result (the dashed red line) is approximately 5–10 K higher than their result (the dashed blue line). The corresponding values of κ_T for isobars of 1 and 1000 bar are shown in Fig. 2. The isobars of κ_T (black circles) obtained from the compressibility equation $\kappa_T = S_{ss}(k = 0)/n_s^0 k_b T$ are slightly higher than those evaluated from the volume fluctuation by Abascal and Vega[28] (red triangles), and in addition, the maximum values provided by our result are located at higher temperatures. Our estimate of C^* is also close to the estimate for a thermodynamic state at T_c = 190 K, n_c^0 = 1.03 g cm^{-3}, and P_c = 1750 bar by Paschek *et al.*[29] using a replica exchange MD simulation with the TIP4P-Ew water model. The overall isobar diagram shown in Fig. 1 agrees with that presented by Paschek *et al.*,[29] although the temperature and density of each isobar determined from our MD simulation with the TIP4P/2005 model are approximately 10 K and 0.01 g cm^{-3} lower, respectively, than those determined with the TIP4P-Ew model. However, we cannot confirm whether the hypothesis of the liquid–liquid transition is valid because we have not confirmed whether the high- and low-density sides are in chemical equilibrium.

Fig. 3 shows the radial distribution function of the oxygen site $g_{ss}(r)$ and the structure factor obtained from $S_{ss}(k) = 1 + n_s^0 \hat{h}_{ss}(k)$, where $\hat{h}_{ss}(k)$ is the Fourier transform of $h_{ss}(r) = g_{ss}(r) - 1$ and n_s^0 is the number density of water. The functions $g_{ss}(r)$ and $S_{ss}(k)$ at 1 bar for 160–300 K are summarized in Fig. 3(a) and 3(b), respectively; those at 3000 bar are shown in Fig. 3(c) and 3(d). The isobars of 1 and 3000 bar in the density–temperature plane are indicated in Fig. 1 as the blue and red circles, respectively. We can see in Fig. 1 that the 1 and 3000 bar isobars tend toward the LDL and HDL side, respectively, with a decrease in the temperature below about 180 K. In Fig. 3(a), we find that both the first and second peaks increase and the first minimum decreases with a decrease in temperature. The change in $g_{ss}(r)$ shows that water molecules located at radial distances around the first minimum between 0.3 and 0.4 nm are moving to radial distances associated with the first and second maxima in $g_{ss}(r)$ so that they form tetrahedral hydrogen-bond networks. The temperature dependence of the structure as seen in $g_{ss}(r)$ should qualitatively correspond to the temperature dependence of the characteristic first and second peaks in $S_{ss}(k)$ shown in Fig. 3(b). As the temperature decreases, the first and second peaks increase

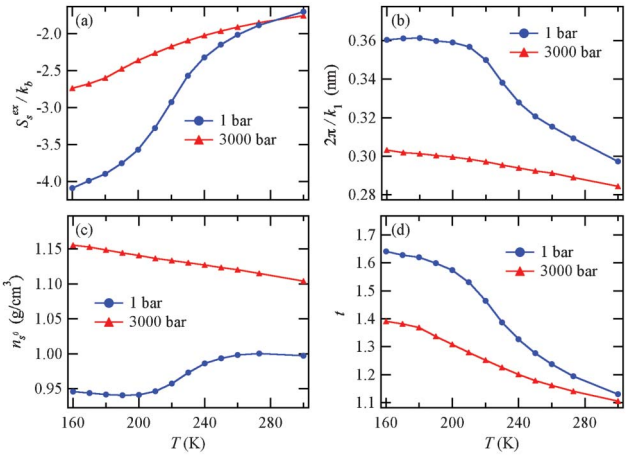

Fig. 4 (a) The excess entropy of bulk water S_s^{ex} from the two-body contribution $S_s^{(2)}$; (b) the spacing between water molecules $2\pi/k_1$, where k_1 is the wave number at the first maximum of $\hat{h}_{ss}(k)$; (c) the number density of water n_s^0; and (d) the translational order parameter t as a function of temperature along isobars of 1 bar (blue circles) and 3000 bar (red triangles).

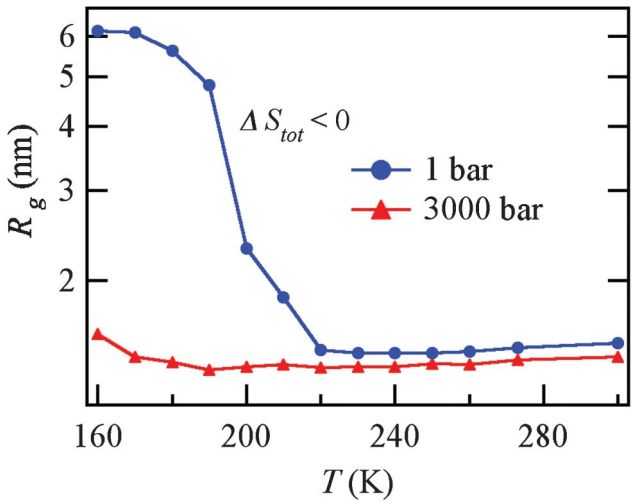

Fig. 5 Radius of gyration of the polymer chain as a function of temperature along isobars of 1 bar (blue circles) and 3000 bar (red triangles).

and their peak positions shift toward small and large values of k, respectively. In comparison with the low-density side at 1 bar, the first and second peaks of $g_{ss}(r)$ at 3000 bar are not as significant, and the position of the second peak of $g_{ss}(r)$ is located at a smaller radial distance at 3000 bar even though the temperature is sufficiently low [see Fig. 3(c)]. This observation suggests that the tetrahedral hydrogen-bond network is distorted on the high-density side at 3000 bar.

In Fig. 4, the temperature dependence of the excess entropy of bulk water S_s^{ex}, spacing between the water molecules $2\pi/k_1$, number density of water n_s^0, and translational order parameter t are shown as a function of temperature along isobars of 1 (blue circles) and 3000 bar (red triangles). The excess entropy of bulk water S_s^{ex} was estimated approximately from the following two-body contribution $S_s^{(2)}$, (ref. 30)

$$S_s^{(2)} = -2\pi n_s^0 k_b \int dr r^2 \{g_{ss}(r)\ln[g_{ss}(r)] - [g_{ss}(r) - 1]\}. \quad (6)$$

The wave number k_1 in $2\pi/k_1$ is that at the first maximum of $\hat{h}_{ss}(k)$. The translational order parameter t was determined from the following definition:[31]

$$t = \int ds |g_{ss}(s) - 1|, \quad (7)$$

where the dimensionless variable $s = r(n_s^0)^{1/3}$ is the radial distance r scaled by the mean intermolecular distance $(n_s^0)^{-1/3}$. In Fig. 4(a), S_s^{ex} along the 3000 bar isobar monotonically decreases as the temperature decreases. This decrease in S_s^{ex} is interpreted as a decrease in the free-volume effect on S_s^{ex} due to the monotonic increase in n_s^0 along the isobar, as shown in Fig. 4(c). In contrast, S_s^{ex} along the 1 bar isobar decreases significantly when the temperature decreases from 273 K to 200 K even if the free-volume effect contributes to an increase in S_s^{ex} at these temperatures, as shown in Fig. 4(c). The temperature dependence of t, shown in Fig. 4(d), appears to be consistent with the temperature dependence of S_s^{ex}. In Fig. 4(b), the value of $2\pi/k_1$ along the 3000 bar isobar monotonically increases as the temperature decreases, but we find a larger increase in $2\pi/k_1$ along the 1 bar isobar with decreasing temperature at temperatures above 210 K. Both the decrease in n_s^0 and the increase in the spacing between the water molecules specified by $2\pi/k_1$ indicate the formation of a tetrahedral hydrogen-bond network at 1 bar. Therefore, the significant decrease in S_s^{ex} along the 1 bar isobar can be attributed to a reduction in S_s^{ex} caused by the formation of the tetrahedral hydrogen-bond network.

Fig. 5 shows the radius of gyration R_g of the polymer chain as a function of temperature along isobars of 1 bar (blue circles) and 3000 bar (red triangles). Along the 3000 bar isobar, no remarkable change in R_g is observed even if the temperature decreases from 300 K to 160 K. On the other hand, a significant increase in R_g is seen in the case of the 1 bar isobar with a decrease in temperature below 220 K. These results suggest that the HDL and LDL are poor and good solvents for the hydrophobic polymer chain, respectively. The difference in the entropies of a globule and swelling state ΔS_{tot} is negative at temperatures below 220 K because $d(\Delta G_{tot}) = -dT\Delta S_{tot}$ is negative with decreasing temperature along the 1 bar isobar, where ΔG_{tot} is the difference in the Gibbs free energy of the globule and swelling states. The physical origin of the negative ΔS_{tot} value is discussed in relation to Fig. 7. The polymer behavior is in accordance with the expectations based on a decrease in the hydration free energy of a small apolar solute examined in supercooled water using MD simulations with the TIP5P-E water model.[32] A similar swelling behavior was demonstrated in a solvent model whose particles interact *via* a two-ramp spherically symmetric Jagla potential.[15,17] The results presented here are consistent with the possibility that the Jagla fluid exhibits water-like solvation thermodynamics

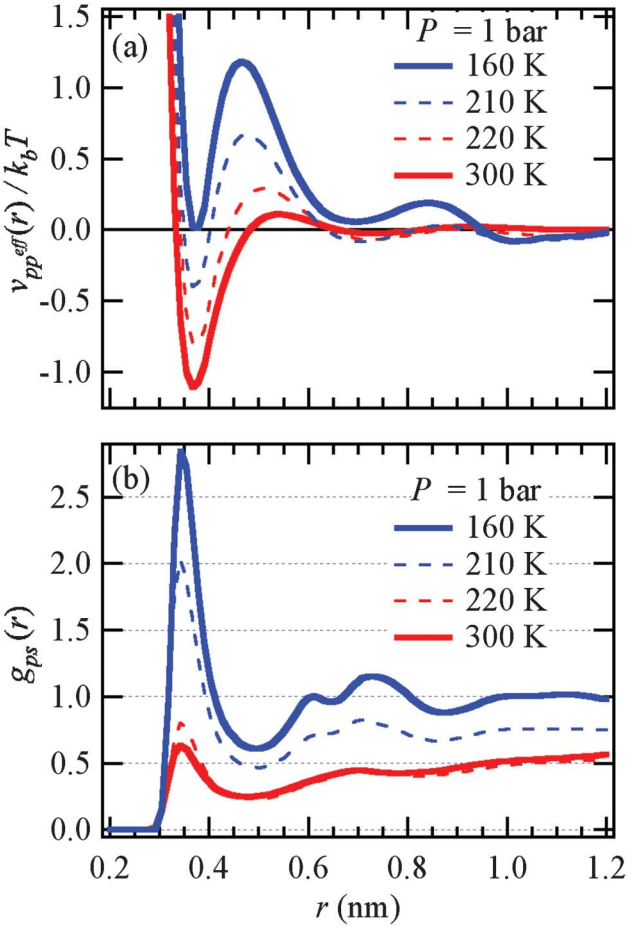

Fig. 6 (a) Effective solvent-induced interaction potential between monomers $V_{pp}^{eff}(r)/k_bT$ for various temperatures at 1 bar, where k_b is the Boltzmann constant. (b) Radial distribution function of water around monomers $g_{ps}(r)$ for various temperatures at 1 bar.

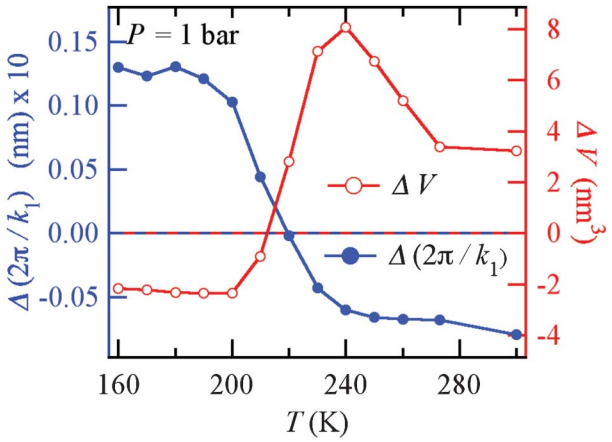

Fig. 7 (Left axis) Change in the spacing between water molecules in the hydration shell due to swelling of the polymer chain $\Delta(2\pi/k_1) = 2\pi/k_1$[swollen] $- 2\pi/k_1$[collapsed] as a function of temperature along the isobar of 1 bar, where k_1[swollen] and k_1[collapsed] are wavenumbers at the maximum in the Fourier transform of $h_{ps}(r) = g_{ps}(r) - 1$ calculated by assuming swollen and collapsed conformations, respectively. (Right axis) Change in volume due to swelling of the polymer chain $\Delta V = V^{ex}$[swollen] $- V^{ex}$[collapsed] as a function of temperature along the isobar of 1 bar, where V^{ex}[swollen] and V^{ex}[collapsed] are the excess partial molar volumes calculated from $-\int \mathbf{dr} h_{ps}(r)$ by assuming swollen and collapsed conformations, respectively. Conformations of the polymer chain at 160 and 300 K were employed as the swollen and collapsed conformations in the calculations of $g_{ps}(r)$, respectively.

for solvophobic polymer chains. However, we realize a discrepancy between the swelling of the polymer chain and cold denaturation of proteins: the swelling transition of the polymer chain takes place at temperatures lower than not only the melting temperature of the water model TIP4P/2005 (about 251 K)[20,33,34] but also the temperature of the maximal growth rate of hexagonal ice for the water model (about 241 K).[34] The swelling phenomenon of the hydrophobic polymer chain is interpreted as being affected by the hypothesized liquid–liquid transition.

In Fig. 6(a) and 6(b), the effective solvent-induced interaction potential between monomers $v_{pp}^{eff}(r)/k_bT$ and the radial distribution function of water around the monomers $g_{ps}(r)$ for various temperatures at 1 bar, respectively, are shown. At 300 K, $v_{pp}^{eff}(r)/k_bT$ has a large first minimum at the monomer contact distance, whereas no distinct minima are observed at radial distances larger than the contact distance. When the temperature decreases to 220 K, the first minimum increases slightly, whereas the second minimum decreases so that water-separated conformations are relatively stabilized. However, a compact globular polymer chain conformation is still stable at 220 K. At both 220 K and 300 K, as seen in Fig. 6(b), water molecules are excluded from the inside of the globular polymer. At 210 K, however, the contact-monomer conformations are significantly destabilized, while the water-separated conformations are stabilized. As a result of the change in $v_{pp}^{eff}(r)/k_bT$, water molecules penetrate the inside of the polymer chain, as seen from $g_{ps}(r)$. For the completely extended conformation at 160 K, both the first and second minima in $v_{pp}^{eff}(r)/k_bT$ become positive, the first maximum becomes higher than k_bT, and the third minimum becomes negative. The $g_{ps}(r)$ function shows that the monomers are strongly hydrated at 160 K. The first and second maxima in $g_{ps}(r)$ at radial distances of 0.34 and 0.61 nm, respectively, are attributed to the first and second hydration shells around a monomer fixed at the origin. The third maximum in $g_{ps}(r)$, meanwhile, can be regarded as the first hydration shell of the nearest-neighbor monomers connected to the monomer fixed at the origin. Three similar maxima in $g_{ps}(r)$ have been observed in a MD simulation of a hydrophobic polymer chain using the TIP5P water model as the solvent.[35] These results, qualitatively comparable with the MD simulation, show the reliability of the DFT model presented here.

Fig. 7 shows the change in the spacing between the water molecules in the hydration shell due to swelling of the polymer chain $\Delta(2\pi/k_1) = 2\pi/k_1$[swollen] $- 2\pi/k_1$[collapsed] as a function of temperature along the 1 bar isobar, where k_1[swollen] and k_1[collapsed] are the wave numbers at the maximum of the Fourier transform of $h_{ps}(r) = g_{ps}(r) - 1$ calculated by assuming swollen and collapsed conformations, respectively.

Conformations of the polymer chain at 160 K and 300 K were employed as the swollen and collapsed conformations in the calculation of $h_{ps}(r)$, respectively; $\hat{\sigma}_{pp}(k)$ determined at 160 K and 300 K were employed as the input for eqn (6). The spacing $\Delta(2\pi/k_1)$ increases slightly as the temperature decreases from 285 K to 240 K. The values of $\Delta(2\pi/k_1)$ at these temperatures are negative, indicating that $2\pi/k_1$[collapsed] is larger than $2\pi/k_1$[swollen]. The spacing $\Delta(2\pi/k_1)$ increases rapidly as the temperature decreases and becomes positive at about 220 K, at which point R_g also starts to increase. The positive value of $\Delta(2\pi/k_1)$ indicates that the spacing between the water molecules surrounding the swollen polymer chain is longer than that surrounding the collapsed polymer chain. In other words, the distortion of the tetrahedral hydrogen-bond network in the hydration shell is relaxed, and a more ideal tetrahedral structure is formed when the polymer chain swells. The decrease in the entropy due to the swelling, *i.e.*, $\Delta S_{tot} < 0$ is, therefore, interpreted as a decrease in the entropy caused by the formation of the more ideal hydrogen-bond network in the hydration shell.

Fig. 7 also shows the change in volume due to the swelling of the polymer chain $\Delta V = V^{ex}$[swollen] $- V^{ex}$[collapsed] as a function of temperature along the 1 bar isobar, where V^{ex}[swollen] and V^{ex}[collapsed] are the excess partial molar volumes calculated from $-\int d\mathbf{r} h_{ps}(r)$ by assuming swollen and collapsed conformations, respectively. The values of ΔV are positive at temperatures above 220 K, whereas ΔV becomes negative when the polymer chain has swollen significantly at temperatures below 210 K. The decrease in the volume due to the swelling, *i.e.*, $\Delta V < 0$, would also contribute to the decrease in the entropy, $\Delta S_{tot} < 0$, owing to the free-volume effect. These observations provide the following physical picture for the hydration shell: Water molecules surrounding the swollen polymer chain attempt to form the more ideal tetrahedral hydrogen-bond network in which the spacing between water molecules is longer but as compact as possible so that the entropy decreases. The thermodynamic stability of the swollen state of the hydrophobic polymer chain $\Delta S_{tot} < 0$ and $\Delta V < 0$ is qualitatively consistent with the thermodynamics of the formation of gas hydrates.

5. Concluding remarks

For the purpose of investigating the relationship between the thermodynamic anomalies of water and the hydration thermodynamics, we performed a multiscale simulation of a hydrophobic polymer chain immersed in water. In this method, the solvation effects on the polymer conformation were taken into account *via* DFT where a free-energy functional model was constructed using the density response function of bulk water and a polymer–solvent pair correlation function, which were determined from MD simulations of bulk water and a DFT-based integral equation for polymer–solvent mixtures, respectively. The multiscale approach overcomes the sampling problems regarding simulations of high-viscosity polymer solutions in the deeply supercooled region.

Isobars determined from the MD simulations using 4000 water molecules and the TIP4P/2005 water model suggest a liquid–liquid transition between the LDL and HDL in the deeply supercooled region. At pressures higher than the hypothesized second critical pressure estimated in the present work, at which the tetrahedral hydrogen-bond network is distorted, the excess entropy of water monotonically decreases in accordance with a monotonous increase in the density of water as the temperature decreases along the isobar. However, at pressures lower than the hypothesized second critical pressure, at which ideal tetrahedral hydrogen-bond networks are formed, the excess entropy decreases significantly with a decrease in the temperature, although a free volume effect due to a decrease in the density of water would contribute to an increase in the excess entropy. The remarkable decrease in the excess entropy on the low-pressure side is therefore attributed to the formation of an ideal tetrahedral hydrogen-bond network that is revealed as an increase in the spacing between water molecules.

Using the multiscale simulation of a hydrophobic polymer chain in water, we investigated the temperature dependence of both the polymer conformation and hydration structure along isobars on the high- and low-pressure sides (1 and 3000 bar). The multiscale simulation approach demonstrated that the polymer chain swells when the temperature is lower than 220 K at 1 bar, *i.e.*, it moves toward the LDL state, whereas no significant conformation change was observed at 3000 bar, even if temperature decreased to 160 K. These results agree qualitatively with reported polymer behaviors in the Jagla solvent model.[15,17] Our theoretical analysis revealed that the entropy-driven swelling of the hydrophobic polymer chain immersed in the LDL that occurs upon cooling is caused by the formation of a hydrogen-bond network in the hydration shells. Moreover, it was also shown that the hydration structures are optimized to reduce the hydration entropy, are as compact as possible, and have a sufficiently large spacing between the water molecules to form a stronger tetrahedral hydrogen-bond network around the swelling polymer chain. These observations are qualitatively consistent with not only an increase in the solubility of small non-polar solutes upon cooling but also a thermodynamic stabilization of clathrate hydrates that trap non-polar compounds inside the cages of hydrogen-bonded water molecules at low temperatures.

Acknowledgements

This work was supported by KAKENHI (Grant-in-Aid for Scientific Research) in the Priority Area ''Soft Matter Physics'' from the Ministry of Education, Culture, Sports, Science and Technology, Japan.

References

1 P. G. Debenedetti and H. E. Stanley, *Phys. Today*, 2003, **56**, 40.
2 J. R. Errington and P. G. Debenedetti, *Nature*, 2001, **409**, 318.
3 P. H. Poole, F. Sciortino, U. Essmann and H. E. Stanley, *Nature*, 1992, **360**, 324.
4 H. Tanaka, *Nature*, 1996, **380**, 328.
5 J. K. Soper and M. A. Ricci, *Phys. Rev. Lett.*, 2000, **84**, 2881.
6 O. Mishima and H. E. Stanley, *Nature*, 1998, **396**, 329.
7 O. Mishima, *Phys. Rev. Lett.*, 2000, **85**, 334.
8 O. Mishima, L. D. Calvert and E. Whalley, *Nature*, 1984, **310**, 393.
9 T. Loerting, C. Salzmann, I. Kohl, E. Mayer and A. Hallbrucker, *Phys. Chem. Chem. Phys.*, 2001, **3**, 5355.
10 E. A. Jagla, *Phys. Rev. E: Stat. Phys., Plasmas, Fluids, Relat. Interdiscip. Top.*, 1998, **58**, 1478.
11 E. A. Jagla, *J. Chem. Phys.*, 1999, **111**, 8980.
12 Z. Yan, S. V. Buldyrev, N. Giovambattista and H. E. Stanley, *Phys. Rev. Lett.*, 2005, **95**, 130604.
13 Z. Yan, S. V. Buldyrev, N. Giovambattista, P. G. Debenedetti and H. E. Stanley, *Phys. Rev. E: Stat., Nonlinear, Soft Matter Phys.*, 2006, **73**, 051204.
14 L. Xu, S. V. Buldyrev, C. A. Angell and H. E. Stanley, *Phys. Rev. E: Stat., Nonlinear, Soft Matter Phys.*, 2006, **74**, 031108.
15 S. V. Buldyrev, P. Kumar, P. G. Debenedetti, P. Rossky and H. E. Stanley, *Proc. Natl. Acad. Sci. U. S. A.*, 2007, **104**, 20177.
16 P. G. Debenedetti, *J. Phys.: Condens. Matter*, 2003, **15**, R1669.
17 S. V. Buldyrev, P. Kumar, H. E. Stanley and S. Weiner, *J. Phys.: Condens. Matter*, 2010, **22**, 284109.
18 T. Sumi and H. Sekino, *Phys. Chem. Chem. Phys.*, 2011, **13**, 15829.
19 T. Sumi and H. Sekino, unpublished.
20 J. L. F. Abascal and C. Vega, *J. Chem. Phys.*, 2005, **123**, 234505.
21 T. Sumi and H. Sekino, *J. Chem. Phys.*, 2005, **122**, 194910.
22 T. Sumi, N. Imazaki and H. Sekino, *J. Chem. Phys.*, 2010, **132**, 165101; T. Sumi, N. Imazaki and H. Sekino, *J. Chem. Phys*, 2010, **132**, 229901.
23 J. P. Hansen and I. R. McDonald, *Theory of Simple Liquids*, Academic Press, London, 2nd edn, 1986.
24 M. P. Allen and D. J. Tildesley, *Computer Simulation of Liquids*, Claredon Press, Oxford, 1987.
25 B. Hess, C. Kutzner, D. van der Spoel and E. Lindahl, *J. Chem. Theory Comput.*, 2008, **4**, 435.
26 P. J. Rossky, J. D. Doll and H. L. Friedman, *J. Chem. Phys.*, 1978, **69**, 4628.
27 J. W. Ponder, *TINKER: Software Tools for Molecular Design*, v. 3.9 2001.
28 J. L. F. Abascal and C. Vega, *J. Chem. Phys.*, 2010, **133**, 234502.
29 D. Paschek, A. Rüppert and A. Geiger, *ChemPhysChem*, 2008, **9**, 2737.
30 Z. Yan, S. V. Buldyrev and H. E. Stanley, *Phys. Rev. E: Stat., Nonlinear, Soft Matter Phys.*, 2008, **78**, 051201.
31 Z. Yan, S. V. Buldyrev, P. Kummer, N. Giovambattista, P. G. Debenedetti and H. E. Stanley, *Phys. Rev. E: Stat., Nonlinear, Soft Matter Phys.*, 2007, **76**, 051201.
32 D. Paschek, *Phys. Rev. Lett.*, 2005, **94**, 217802.
33 R. G. Fernández, J. L. F. Abascal and C. Vega, *J. Chem. Phys.*, 2006, **124**, 144506.
34 D. Rozmanov and P. G. Kusalik, *Phys. Chem. Chem. Phys.*, 2011, **13**, 15501.
35 D. Paschek, S. Nonn and A. Geiger, *Phys. Chem. Chem. Phys.*, 2005, **7**, 2780.

